Scientific report; WR-2002-04

KNMI

Assimilation of satellite derived surface heating rates in a Numerical Weather Prediction Model

Bart van den Hurk and Han The

Koninklijk Nederlands Meteorologisch Instituut

De Bilt, 2002

Scientific report = Wetenschappelijk Rapport; WR 2002-04

De Bilt, 2002

PO Box 201, 3730 AE De Bilt
The Netherlands
Wilhelminalaan 10
http://www.knmi.nl
Telephone +31 30 22 06 911
Telefax +31 30 22 10 407

Authors: Hurk, Bart van den
The, Han

UDC: 551.507.362.2
551.509.313
551.577

ISSN: 0169-1651

ISBN: 90-369-2214-3

Assimilation of satellite derived surface heating rates in a Numerical Weather Prediction model

Bart van den Hurk and Han The

KNMI

PO Box 201

3730 AE De Bilt, The Netherlands

August 2002

Abstract

In a simplified data assimilation scheme, surface temperature heating rates were used to adjust the soil moisture content in the limited area atmospheric model RACMO. These heating rates were derived from the geostationary METEOSAT satellite IR clear sky pixels after sunrise. In this paper we will discuss the applied cloud detection algorithm, atmospheric correction, specifications of the observation error and the formulation of the data assimilation method. Further, a case study applying the scheme here described will be presented, extending over the Southern and Central parts of Europe between 1 May and 1 October 2000. Comparison of the model results and a large number of observed 2m temperatures at synops locations revealed a small but systematic improvement in the central part of Europe, but a slight deterioration over the Iberian peninsula. To some extend, this might be related to the uniform specification of the aerodynamic coupling between the surface and the atmosphere within the model. Altogether, we may conclude that satellite data contain a useful additional signal to correct model soil moisture content and aerodynamic parameters simultaneously.

1. Introduction

The models forecast used for Numerical Weather Prediction (NWP) critically depends on the initial conditions of the prognostic fields. This does not only apply for initial atmospheric fields, but also for the state of the land surface and soil (Viterbo, 1996). Being slow components in the cycles of energy and water, soil temperature and moisture content are susceptible for accumulating systematic errors in the representation of these cycles. This can lead to serious drifts of the NWP system in spite of the atmospheric data assimilation (Viterbo and Courtier, 1995). For that reason, various NWP centres across the world apply data assimilation procedures to constrain errors in the soil prognostic quantities. Usually, diagnosed forecast errors in near-surface air temperature and/or humidity are used, assuming they contain information about the surface energy budget under conditions where land surface and atmosphere are closely coupled (Mahfouf, 1991; Bouttier et al, 1993a, 1993b; Giard and Bazile, 2000; Douville et al, 2000; Rhodin et al, 1999; Hess, 2001). However, this coupling is often weak or is strongly determined by the amount of available radiative energy at the surface. Observations of this net radiation are not included in the data assimilation scheme. Moreover, the density of the observation network of near surface quantities is often sparse. Therefore, in many areas such as the (semi-)arid areas in the subtropics and continental Asia this approach will fail at all, whereas in these regions constraining soil moisture and/or air temperature are even more important (see e.g. Koster et al, 2000, for an analysis of the geographical distribution of significant land-atmosphere feedback).

Satellite observations of the land surface might fill this gap. Studies with a range of existing and future satellite microwave instruments have been carried out, and there is increasing confidence that these measurements can be assimilated into land surface schemes of NWP models. In particular, observations in the L-band (1-4 GHz) contain useful signal (Houser et al, 1998; Calvet et al, 1998; Wigneron et al, 1999). It was shown, for example, that there is a direct physical relation between top soil moisture content and the emission or reflection of microwave radiation at frequencies ranging from 1 to 20 GHz (e.g. Wigneron et al, 2000). Although satellite programs (SMOS; Hydrostar) aiming to provide these observations are underway, at the present no such data are available on an operational basis. Instead of directly quantifying the top soil moisture from satellite data we used an indirect method estimating the top soil moisture from measured surface heating rates.

There is an intuitive relation between heating rates and soil moisture content. We may expect higher heating rates if soils are dryer and vise versa. Unfortunately, this relation is not fixed. Not only does it depend on the soil properties, it also depends on the energy exchange with the atmosphere. Currently, there are two types of approach to this problem: the turbulent surface fluxes are estimated using thermal and visible data (e.g. Bastiaanssen et al, 1997; Van den Hurk et al, 1997; Menenti and Choudhury, 1993), or the rate of change of surface temperature after sunrise is related to the surface energy budget, the so-called heating rate method (Wetzel et al, 1984; McNider et al, 1994; Jones et al, 1998a,b). A review of these methods was given by Van den Hurk (2001). These methods have in common that the partitioning of net radiation over sensible and latent heat flux at the land surface leaves its marks in the surface temperature. This provides a relation between the moisture status of the soil (affecting the surface radiation partitioning) and the surface temperatures observable from space. This relation is sensitive to the amount of radiation reaching the surface (partially determined by the shortwave reflectance), the presence of vegetation, and the aerodynamic properties of the surface and of the atmospheric flow. Relying on surface temperature observations, atmospheric conditions (clouds, aerosols) form a clear constraint on the observations.

This paper describes a potential pre-operational implementation of the heating rate method for soil moisture data assimilation for Europe, making use of routine observations of the geostationary METEOSAT satellite. First, we explain the principles of the scheme, the preparation for the observations, and the assimilation in a NWP land surface model. Next, we will present results of a case study using the RACMO model (Christensen et al., 1996) to assess the impact of the data assimilation using near-surface temperature observations as verification material. The study covers a five month growing season in 2000. The final section will discuss the outlooks on the practical implementations of the scheme. Note that satellite data are merely indicative to the top soil moisture. Deep soil moisture could be estimated only when using more complex soil models using the top soil moisture as a boundary condition.

2. Method and observations

This section describes the principles of the heating rate method, how we determined the heating rates using satellite observations as well as a NWP model, and the specification of parameters related to the data assimilation. A final subsection describes the case study employed.

2.1. The heating rate method and principle of the data assimilation procedure

The heating rate method (Wetzel et al, 1984; McNider et al, 1994) relates the rise of the surface temperature after sunrise to the partitioning of net radiation at the surface and to the thermal inertia of the top soil. The net radiation received at the land surface is absorbed by the soil and vegetation, which results in a temperature rise. This temperature increase gives rise to the exchange of heat with the atmosphere and the underground. Turbulent exchange of latent heat with the atmosphere is associated with a surface temperature cooling, caused by the phase change of liquid water into water vapour. Therefore, cases where substantial amounts of energy are released as latent heat, the surface temperature increase with increasing net radiation is less than under dry conditions (see Figure 1). This is the basic principle of the heating rate method.

The heating rate is further affected by the thermal inertia of the soil-vegetation system, determining the delay of the surface temperature change with respect to the temporal signature of the net radiation. This thermal inertia causes a general hysteresis effect when a direct relation between net radiation and surface temperature is evaluated (Figure 1). Finally, an important factor affecting the surface temperture change as a function of the received amount of net radiation is the (aerodynamic) coupling of the surface to the atmosphere and the (thermodynamic) coupling to the underlying soil. These coupling processes are usually accounted for by variable exchange coefficients in land surface modules of NWP systems. These exchange coefficients govern the The magnitudes of heat release of the surface. High barriers to energy exchange with both the atmosphere (e.g. under conditions of low wind speeds or strong atmospheric stability) and the underground (low thermal conductivities in dry soils or tall vegetation) will lead to higher surface temperatures than under conditions of rapid energy exchange. Furthermore, depending on the ability of vegetation to transpire, the aerodynamic exchange coefficient may play an important role in partitioning the net radiation in sensible and latent heat.

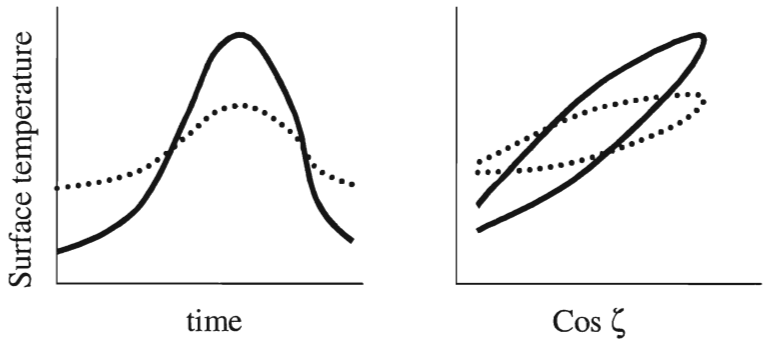

Figure 1: Principle of the heating rate for a dry surface (solid lines) and a wet surface (dotted lines). Left the diurnal courses are shown, right the surface temperature as function of the cosine of the solar zenith angle, showing the delaying effect of the thermal inertia of the soil.

McNider et al (1994) and Jones et al (1998a,b) designed and applied procedures in which the observed heating rate is related to the processes briefly listed above. Estimating soil moisture content was their primary objective, and they eliminated or estimated the remaining unknown quantities in the system by inserting ancillary data on vegetation, soil physical characteristics and aerodynamic properties in a (calibrated) land surface parameterization (LSP) scheme. They used prescribed relationships between soil moisture content on the one hand, and coefficients of canopy transpiration, soil evaporation and the soil thermal inertia on the other, to define the soil moisture content to obtain an optimal match between observed and modelled surface heating rate (Figure 2). By definition, the soil moisture content thus obtained is a model quantity forcing the LSP to the observed heating rate. It is sensitive to assumptions regarding its role in regulating canopy transpiration, soil evaporation and the soil thermal inertia. Errors in these assumptions are likely to deteriorate a verification using in situ soil moisture data, in spite of the fact that the LSP may give a perfect simulation of the surface heating rate. Soil moisture products generated by this data assimilation procedure are therefore closely related to the underlying LSP, and generally it should not be compared to field data or results from LSP's that are formulated differently as such.

In the current study we have roughly followed the data assimilation procedure outlined above. The surface heating rate was calculated using a land surface model based on the recently updated scheme by Viterbo and Beljaars (1995) (see next subsection), implemented in a limited area NWP model. The multi-layer soil moisture content in the LSP was varied according to a minimization procedure in order to improve the match between observed and modelled surface heating rates.

The data assimilation procedure is a simplified variational minimization scheme, in which a cost function J that measures the distance between observed and modelled quantities, is defined:

$$J = \sum_i \frac{\left(x_{m,i} - x_{o,i}\right)^2}{\sigma_{o,i}^2} + \sum_j \frac{\left(\Delta w_j\right)^2}{\sigma_{w,j}^2} \qquad (1)$$

where $x_{o,i}$ is the collection of observed quantities (i.e. the satellite derived surface heating rate), $x_{m,i}$ the modelled equivalence, and $\sigma_{o,i}$ the observation error (see Section 2.4). The second term in Eqation 1 determines the penalty of modifying the model variables w_j (denoting the soil moisture content here) by an increment Δw_j, relative to a so-called background error $\sigma_{w,j}$. The observation error of each observed quantity, $\sigma_{o,i}$, and the background error of each

modified model variable, σ_{w_j}, need to be defined in advance. $\sigma_{o,i}$ and $\sigma_{w,j}$ express the confidence levels for the observations and the unmodified (first guess) model estimate, and, consequently, their ratio is the prime quantity that determines the range within which the observations may affect w_j.

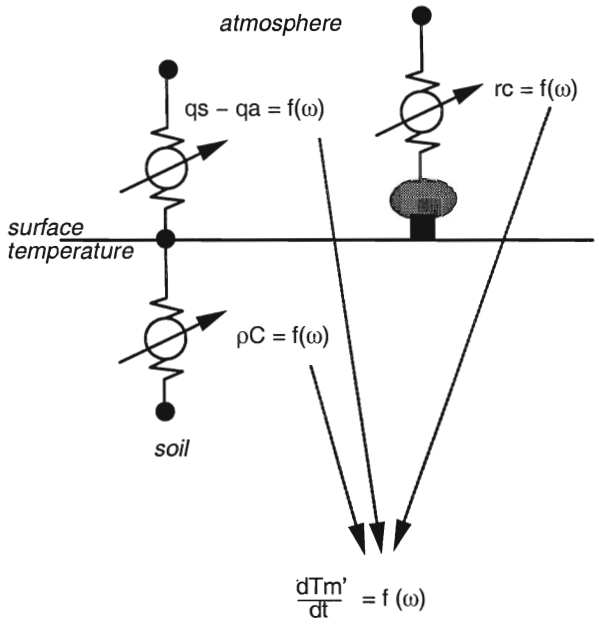

Figure 2: Principle of the data assimilation procedure. Soil moisture content ω affects the thermal inertia of the top soil (ρC), the soil evaporation (governed by humidity gradient $q_s - q_a$*), and the canopy resistance against transpiration* r_c*. An optimal value of soil moisture content is defined by the closest match between observed and modelled surface heating rate.*

Expression J was minimized using a simplified Newtonian search scheme (Hess, 2001). Near the optimum, $\partial J/\partial w_j$ is assumed to be linear to Δw_j for each $j = 1,\ldots, n$. This implies that the minimum of J can easily be found by a finite difference gradient determination, requiring one additional simulation with the forecast model for each quantity w_j to be optimized.

Theoretically, corrections to w in a given model grid box may affect the heating rate of adjacent gridboxes in the domain. However, the coupling between the surface heating rate of a grid box and the soil moisture content within that grid box is generally much stronger than the coupling to soil moisture content in adjacent grid boxes. Therefore, horizontal correlations between increments of w and changes of heating rates outside the grid box may be ignored (Rhodin, 1999). This reduces the optimization problem of Equation 1 to a system where only $n + 1$ integrations are needed: a first guess estimate starting from the previous values of w, and n integrations with small perturbations of w_j with $j = 1,\ldots,n$. From these integrations a value for J is found that minimizes the difference between the observed and simulated heating rate taking the model accuracy into account. The derivation of the observed and simulated heating rate is discussed below.

2.2. Derivation of the observed heating rate

The surface heating rates were derived from METEOSAT infrared measurements. For several reasons the measured infrared temperatures do not represent the actual surface temperature. Thin cirrus cloud and sub-pixel clouds cannot be detected simple, but their effect on the measured change of temperatures can be significant. Mainly due to this cloud contamination, the heating rates cannot be determined by simply deducting the infrared temperatures of two subsequent images. Even for genuinly cloud free pixels we are not sure about the surface temperatures, because the

moisture in the atmosphere affects the upwelling radiation, requiring so-called atmospheric correction. In this section we will discuss how to tackle these problems.

Definition of the heating rate

The primary energy source leading to the increase of the surface temperature T_s after sunrise is solar short wave radiation. Assuming a quasi-linear relation between incoming solar radiance and surface temperature, we can get rid of the temporal temperature tendency for seasonal and spatial solar variations. The incoming radiance equals $I_e \tau cos\zeta$, where ζ is the solar zenith angle and I_e the extraterrestrial radiation and τ the transmissivity. $\partial T_s/\partial t$ tends to decrease during the day. Therefore, rather than defining the heating rate as a temporal tendency, we will use the expression Υ instead, defined as:

$$\Upsilon = \frac{\partial T_s}{\partial \cos \zeta} \qquad (2)$$

Major advantage of using Υ instead of $\partial T_s/\partial t$ is its linearity (as a first approximation), implying that its value can be determined from time series by linear regression more accurately than $\partial T_s/\partial t$. Note that, consequently, Υ is fairly constant throughout the morning hours, except for the early hours after sunrise, when τ is changing rapidly. Hence, the period of time to determine Υ is less critical than would be the case for $\partial T_s/\partial t$. Hence, there is no need to use a fixed time for Υ. Due to hysteresis, Υ does not have any meaning after midday (the cooling curve does not match the heating curve). Υ was determined within a time frame of 2 hours after local sunrise and 11:00 am local solar time.

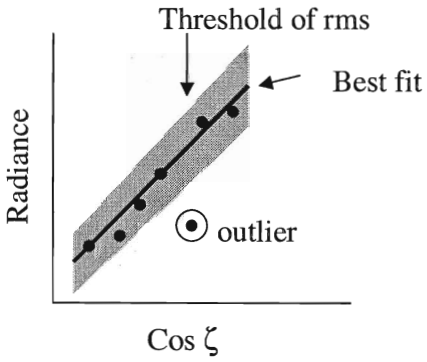

Figure 3: Principle of the cloud detection algorithm, showing a linear fit of the observed radiance as function of cos ζ. The shaded area represents the threhold of the tolerable rms. The outlier from this range is detected as being cloudy.

Cloud detection

Accurate heating rate detection requires cloud free conditions during a sufficiently long consecutive period in the sampling interval. Various cloud detection algorithms based on instantaneous satellite observations exist (e.g. Feijt et al, 2000). Major restriction of these algorithms is that they do not analyse the images as a time series. Consequently, it is impossible to detect deviations of a few degrees in the infrared due to cloud contamination. These deviations are of the same magnitudes as the heating rates themselves. Therefore we applied a more restrictive, but internally consistent cloud detection procedure (see Figure 3).

Using times series of both infrared and visible light METEOSAT images, as well as their spatial variation offer enough information to exclude any trace of cloud contamination. Cloud-free conditions during moring hours can be associated with both positive heating rates (IR) and increasing VIS intensities. Departing from these conditions and threshold values for the residual error of the linear regressions serve as criteria to detect outliers of data points. The threshold values of the residual errors were evaluated using a large set of METEOSAT pixels co-located with synops observations of total cloud cover, serving as ground truth. Points resulting in rms errors exceeding these thresholds were removed. In addition, the VIS images were compared with the clear sky reflections derived from a long time period of METEOSAT images. Locations where during less than two consecutive hours cloud-free pixels were detected were flagged as permanently cloudy pixels and not used in the data assimilation.

A combination of temperature and reflectance observations results in a rather conservative but robust algorithm. Figure 4 shows a summary of a comparison of the current detection algorithm to results obtained using the so-called MetCLOCK algorithm (Feijt et al, 2000). MetCLOCK uses a thresholding of instantaneous surface temperature and reflectance measurements. Thresholds are calibrated using observed cloud cover at synops stations, and vary in time and space. A significant consistency in the cloud detection was found. However, a substantial amount of pixels are flagged as being cloudy whereas MetCLOCK labeled these as cloud-free. Reversely, only a limited number of pixels passed the cloud-detection where MetCLOCK would label these as cloudy.

Figure 4: Example of a comparison of the current cloud detection algorithm with the MetCLOCK algorithm of Feijt et al (2000). Pixels are coloured according to the consistency with MetCLOCK: Light grey: both cloudy; light middle grey: MetCLOCK cloud free, present algorithm cloudy; dark middle grey: both cloud free; dark grey: MetCLOCK cloudy, present algorithm cloud free.

Atmospheric correction

In contrast to the implementation of the heating rate method by McNider et al (1994), we applied atmospheric correction to the infrared images. Muller et al. (1990) clearly demonstrated a strong dependence of the atmospheric distortion on the surface temperature itself. The atmosphere is slightly opaque in the infrared due to water vapour in

the atmosphere. Consequently, the top-of-atmosphere (TOA) temperature, as measured by the satellite, is generally lower than the surface temperature. An increase of the surface temperature will not be lead to the same increase in the TOA temperature. This deviation induces a clear diurnal cycle of the atmospheric correction, which can be as large as 1-2 degrees Kelvin per hour in Southern Europe; i.e. about the same magnitude as the surface heating rate itself.

The atmospheric corrections were calculated using the MODTRAN 4 radiative transfer model. Actually, one does not calculate the atmospheric correction itself, but determines the surface temperature iteratively, using the TOA temperature as a boundary condition. The atmospheric correction is given by the difference between TOA and T_s. The input atmospheric profiles were obtained from the first guess simulations of the NWP model (see below). Constraints on computer power hampered a pixel-by-pixel calculation for each METEOSAT image. Therefore, we restricted the MODTRAN calculations to the (coarse) resolution of the NWP model. At each grid point we calculated the TOA temperature for three different values of T_s to obtain a functional relation between TOA temperature and T_s, $T_s = T_s(T_{toa})$, hence avoiding time consuming iterations. The corrections per pixel were determined by spatial interpolation between these functions. Furthermore, we did not calculate the atmospheric corrections for all images either. We first estimated the TOA temperature as a linear function of $cos\zeta$, similar to Equation 2, by applying linear regression on the raw METEOSAT IR clear sky data. Assuming that the atmospheric correction is proportional to the TOA temperature, we transformed this relation to a linear relation between T_s and $cos\zeta$ by calculating the atmospheric correction for two time slots only.

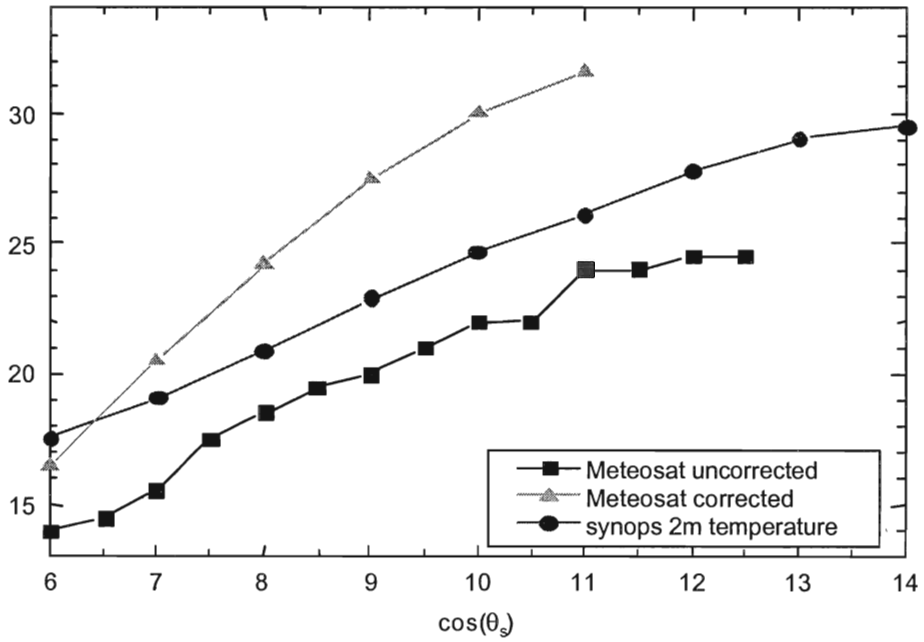

Figure 5: Example of the impact of the atmospheric correction. Shown is a timeseries of uncorrected and corrected surface temperature, in combination of co-located observations of air temperature at 2 m.

Figure 5 provides a typical example of the impact of the atmospheric correction on the surface temperature. It shows the timeseries for a cloudfree pixel during a summer morning. The uncorrected surface temperature is lower than the air temperature during the entire period, whereas the corrected surface temperature shows the expected behaviour of

being lower than the air temperature during early morning, and increasingly exceeding the air temperature during later times. Obviously , ignoring the atmospheric correction would lead to significantly different heating rates.

2.3. Calculation of the heating rate in the atmospheric model

Many land surface models define the surface temperature as the temperature of a soil layer of finite depth with a certain heat capacity (e.g., Gustafsson et al, 1993). Its thickness and thermal inertia are usually tuned to be able to resolve surface temperature variations at the diurnal scale, but they are incapable of representing rapid temperature changes associated with for instance cloud overpasses, advection of air mass changes or the influence of precipitation. Therefore, a so-called skin temperature was introduced, defined as the temperature that closes the instantaneous surface energy balance. As such, the skin layer associated with this temperature has no heat capacity and can vary rapidly with changing environmental conditions (e.g. Viterbo and Beljaars, 1995). At the characteristic resolution of NWP models (20 – 50 km) substantial variability of the surface temperature may be encountered as a result of variability in surface (vegetation) cover, orography and soil wetness. To account for this variability, an increasing number of surface schemes adopt the concept of tiling (e.g. Koster and Suarez, 1992) in which separate energy balance calculations are carried out for various subfractions of a grid box with more or less homogeneous properties.

In our NWP model we implemented a new version of the land surface scheme from the European Centre for Medium-Range Weather Forecasting (ECMWF). This land surface model is a tiled version of the scheme designed by Viterbo and Beljaars (1995). Its structure and verification using field data are briefly described by Van den Hurk et al. (2000). The surface temperature is defined as a composite of the skin temperature from six subgrid fractions (low vegetation, high vegetation, intercepted water, bare ground, snow on low vegetation, snow under high vegetation), whose areal coverage varies as a function of vegetation type distribution, snow evolution and amount of precipitation intercepted by canopies. Each of these subgrid fractions has a specific thermal and hydrological coupling to the soil and to the atmosphere. In each NWP gridbox, one skin temperature is calculated as an areal weighted average of the skin temperatures of these fractions. This average temperature is used to calculate the surface heating rate in the NWP model.

The direct comparison of satellite derived and modelled surface skin temperatures (and their rates of change) is hampered by a potential inconsistency between the satellite-based observations, and the NWP definition of skin temperature. The NWP skin temperature is dominated by an aerodynamic coupling of the surface to the atmosphere, rather than by the longwave radiative properties of the surface (Sun and Mahrt, 1995). In order to reduce the difference between the observed radiative surface temperature and the NPW skin temperature, many surface models, including the one in this study, introduced a distinction between an aerodynamic (i.e., governed by momentum exchange) and a thermal turbulent exchange coefficient, using a reduced surface roughness length for heat, z_{0h}, and the roughness length adopted for momentum, z_{0m}. Although its ratio, z_{0h}/z_{0m}, is highly variable in time and in space (Verhoef et al, 1997), it is often assumed to be constant. In the ECMWF land surface model, a value of 0.1 was adopted. This might have had a significant impact on the results of this data assimilation study, as will be discussed later.

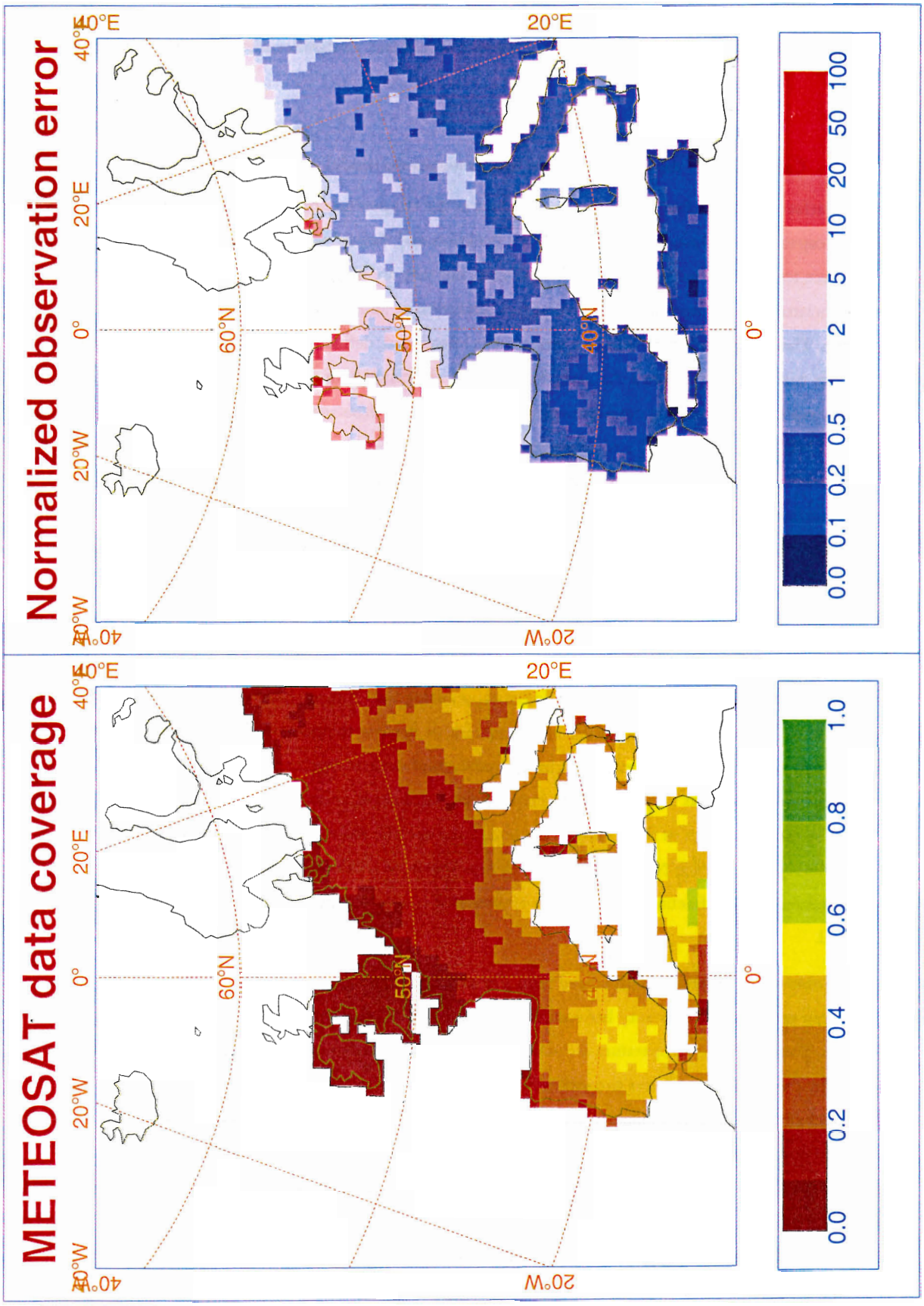

Figure 6: Case sudy area. Left: fraction of days for which valid surface heating rates could be derived from the METEOSAT observations. Right: spatial distribution of the ratio between average observation error and average heating rate between 1 May and 1 October 2000.

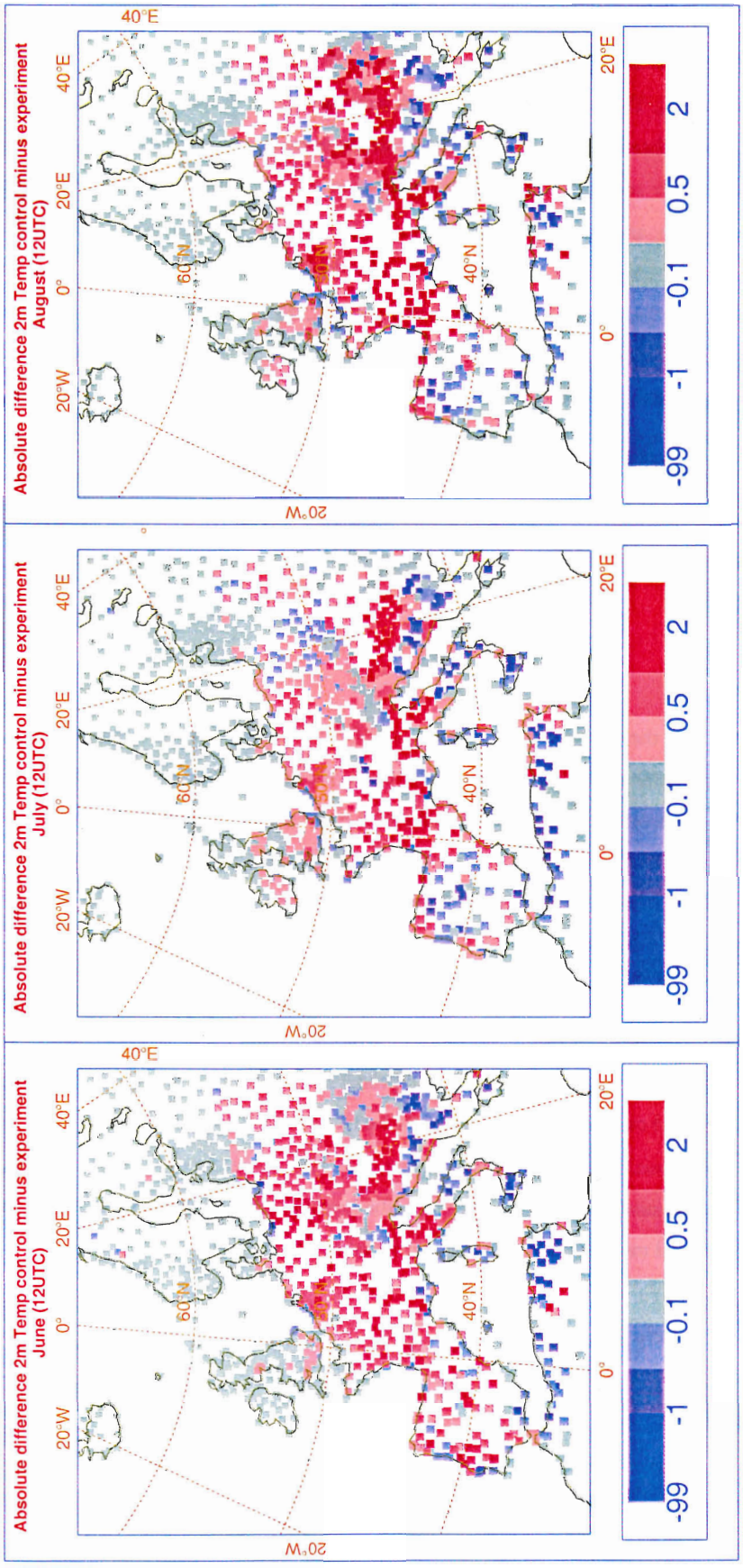

Figure 7: Monthly averaged difference between the absolute biases of 2m temperature at noon of the control simulation and the experimental suite, i.e. $|T_{control} - T_{obs}| - |T_{exp} - T_{obs}|$. *Shown are maps for June, July and August 2000. Values in red show locations where the experimental suite is closer to the observations than the control, blue the reverse. Light blue points denote no change.*

2.4. Definition of observation and background errors

The data assimilation procedure requires a priori estimates of the observation error, σ_o, and a background error of the soil moisture estimate σ_w. The observation error is determined by the accuracy in which the heating rates can be obtained from the satellite observations, which depends on the number of observations, the error in the measured irradiance, inaccuracies in the atmospheric correction procedure, quality of the cloud screening and temporal variability of the atmosphere, and so on. Most of these aspects cannot easily be measured. Largest contribution to σ_o, though, are presumably the subgrid clouds and cirrus clouds which cannot be filtered out; 'cloud free' pixels are most likely to be contaminated by some cloud. Within a model grid cell, the amount of subgrid cloud contamination is assumed, therefore, to be a function of the fraction of cloud free satellite pixels. Furthermore, the variance of observed clear sky heating rates for pixels close together, expressing the spatial variability of heating rates, is fairly small. Although, this variance is also affected by the variability of the land surface characteristics determining surface heating rate, this contribution is smoothed out already by the METEOSAT pixel size (30 km^2 or more at mid-latitude). Although it has not been investigated in detail, we will assume, therefore, that this effect is relatively small. Under this assumption we can express the observation error as:

$$\sigma_o^2 = \frac{\sigma_\Upsilon^2}{f_{cl}} \tag{3}$$

where σ_Υ^2 is the variance of the observed heating rates, and f_{cl} the fraction of cloud-free pixels. σ_Υ^2 and f_{cl} are evaluated using all pixels within a NWP grid box, which forms the primary spatial unit of the generated soil moisture fields. Higher observation errors are produced for areas with either a low number of cloud-free pixels or in areas where the spatial coherence of the observed heating rates is low (see also Van den Hurk et al., in press). Averaged over the simulation domain (see below) the observation error is approximately 20% of the heating rate signal, which is assumed to be a reasonable estimate.

The background error σ_w expresses the accuracy of the soil moisture parameterization scheme, used in the NWP model. It includes the uncertainties in the evolution of precipitation and atmospheric forcing determining the soil moisture content, as well as the parameterization of the processes generating evaporation and water loss due to runoff. In principle, repeated calculation of soil moisture increments contains information on the background error of the soil moisture calculation. However, in this study we have chosen a constant and relatively high value for σ_w^2, in order to evaluate the potential information content in the heating rate observations, i.e. we imposed a small contribution of the modified model variable to the cost function J (Equation 1).

3. A case study

3.1. Description

The case study covers a large portion of Europe during the growing season of 2000. Figure 6 gives an overview of the area for which the data assimilation was carried out. Daily METEOSAT heating rates were derived between 1 May and 1 October 2000. We used METEOSAT data with latitudes below 56°N only, since the viewing geometry and systematic cloud cover yield unreliable surface temperature estimates in more northerly regions. To a large extend, the availabilty of useful data was determined by the occurrence of clouds. In the UK less than 10% of the

days between 1 May and 1 October 2000 were favourable for calculating Υ, against less than 20% in most parts of in the remaining target area. Consequently, the relative observation error shows a gradual increase with latitude, with almost meaningless observations (in terms of signal/noise ratio) in the most northern parts of the domain.

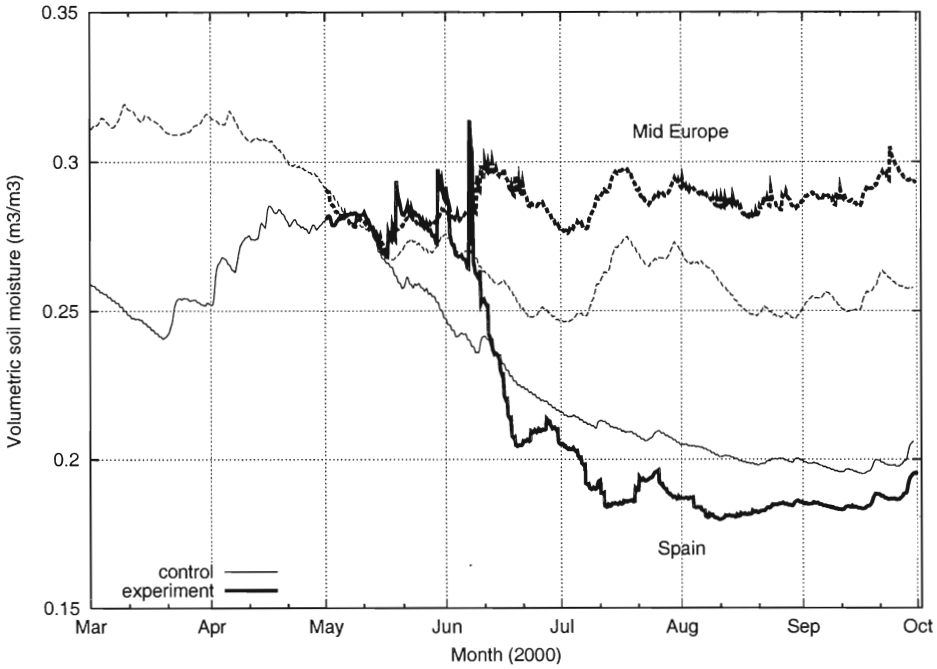

Figure 8: Time series of soil moisture content in the top 1 m of soil for the Iberian peninsula (solid lines) and the mid-European continent (dashed lines) for the control simulation (thin lines) and the experimental suite with soil moisture data assimilation (thick lines).

Model integrations were carried out with RACMO at a grid resolution of approximately 50×50 km, operating in NWP-mode. This implies that simulations are started daily from an initial atmospheric analysis. Initialisation and lateral boundary conditions needed to force the model to follow the observed large scale weather patterns, were obtained from the operational ECMWF global analyses.

A control series of daily RACMO forecasts of 24 hours was initiated on 1 March 2000. Initial soil temperature and soil moisture content were obtained from operational ECMWF soil fields. In most parts of Europe, the initial soil moisture content was close to field capacity, owing to low evaporation losses and frequent supply of winter time precipitation and early snow melt. After initialization, soil moisture and soil temperature evolved freely according to the modelled precipitation, evaporation loss and discharge via runoff. The control series of 24 hours forecasts extended until 1st October 2000.

From 1st May onwards, a second series of RACMO forecasts was carried out, in which METEOSAT heating rates were assimilated. Half-hourly IR temperature fields were used to calculate the average clear sky heating rates between 2 hours after sunrise and 11:00 local time. These data were aggregated to RACMO resolution. The observation error was determined as outlined in Section 2.4.

3.2. Results

The results were tested by compared the air temperatures at 2m height from the operational observation network at 12:00 and 18:00 UTC with both RACMO runs. We used bilinear interpolation between the temperatures at the nearest by RACMO land grid points to the location of the synops station. Differences in height between the

observation point and the RACMO surface level were corrected using a constant lapse rate of 6.5 K/km.

Figure 7 shows the effect of the adjusted soil moisture contents on the 2m temperature at noon. The quantity displayed is the difference between the absolute biases between the observations and the control simulation on the one hand, and the experimental suite on the other: $|T_{control} - T_{obs}| - |T_{exp} - T_{obs}|$. Large positive values indicate that the experimental results are closer to the synops data, whereas negative values point out a worsening. Figure 7 shows the monthly averaged results for June, July and August, which is the period where the soil moisture assimilation has the most pronounced effect on the surface energy balance. We can see a clear improvement over large parts of Western and Central Europe. This improvement is related to a systematically higher soil water content compared to the control run (Figure 8). This leads to higher amounts of energy used for evaporation, thereby reducing the sensible heat release to the atmosphere and a leading to a lower near-surface air temperature. The systematic positive temperature bias in this area is thus reduced by the soil moisture assimilation.

For the Iberian Peninsula the results are more ambiguous than for Central Europe. Systematic improvements are observed at some locations especially near the coast, but for many locations the data assimilation results in deteriorating 2m temperatures. In contrast to the Central European area, on average, the data assimilation procedure is causing a reduction of the soil moisture content. As a result, the 2m temperatures are systematically higher than in the control simulation, implying an increase of an already existing positive bias. The lower soil moisture contents in the experimental suite retained throughout the end of the period (October 2000).

The systematic temperature bias in the control simulation displays a clear diurnal cycle (Figure 9). At 12:00 UTC the data assimilation applied in the experimental suite results in a small but systematic reduction. The effect is most pronounced for the ensemble of synops observations taken in the mid-European area (higher than 40°N), whereas for the Iberian peninsula results are smaller. However, at 18:00 UTC (bottom panel in Figure 9) the temperature changes take the same sign, i.e. a general reduction as a response to added soil water, but the bias of the control model was already generally negative, and is thus enhanced. This diurnal cycle of the temperature at 2m height is believed to be related to other processes than the surface energy partitioning. In the summer months 18:00 UTC is around sunset in a large portion of the Eastern part of Europe. For many stations the temperature at this time is related to the development of a stable boundary layer, for which parameterization difficulties unrelated to soil moisture are of significant importance. Indeed, the temperature bias at 18:00 UTC is related to the geographical longitude of the synops location, being on average approximately zero at 10°W and –2 K at 30°E (Figure 10). At noon no such geographical dependence is evident.

4. Discussion and outlook

The assimilation of satellite derived heating rates in the ECMWF land surface model may lead to a reduction of the 2m temperature bias at noon during the summer months in Western and Central Europe.

This temperature bias contains a clear diurnal cycle, switching from a general positive bias at noon to a negative bias at 18:00 UTC. The late afternoon bias is probably related to the formulation of the stable boundary layer in RACMO, and to possible errors in the longwave radiative cooling resulting from problems with cloud cover simulations. In some operational soil moisture assimilation schemes use is made of synops observations at multiple times per day (e.g. Giard and Bazile, 2000). A diurnal cycle in the temperature bias must be accounted for carefully in order to avoid an artificial diurnal cycle in the soil moisture corrections that are derived from the synops data. The

diurnal cycle in the bias also reveals an additional difficulty with the relatively sparse temporal coverage of generally 4 (or less) observations per day when using synops data for soil moisture assimilation.

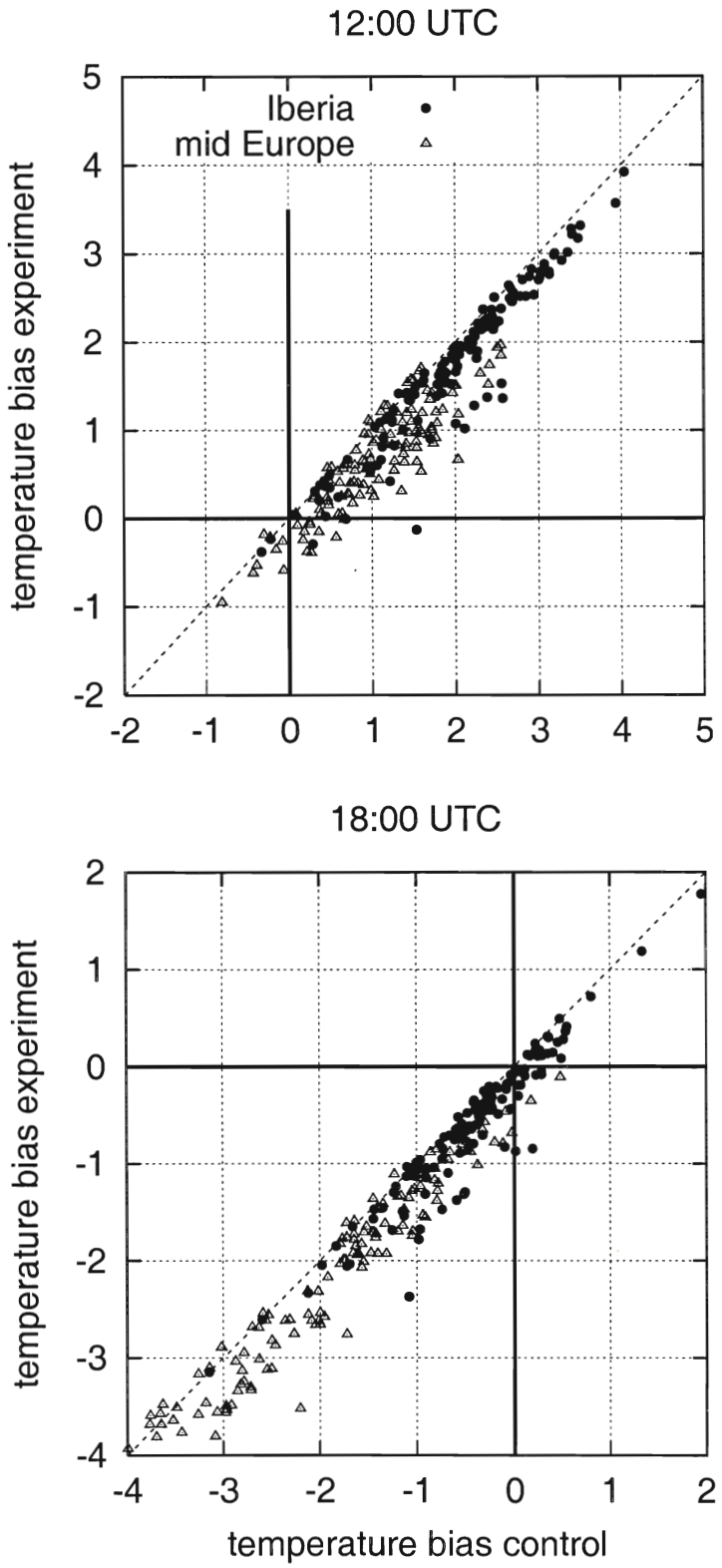

Figure 9: Daily temperature bias in the period between 1 May and 1 October 2000. Each symbol represents the bias on a given day averaged for all synops stations in the mid-European area (triangles) and the Iberian peninsula (closed circles) from the control versus the experimental RACMO simulations. Shown are the bias of temperature at 12:00 UTC (top panel) and 18:00 UTC (bottom panel).

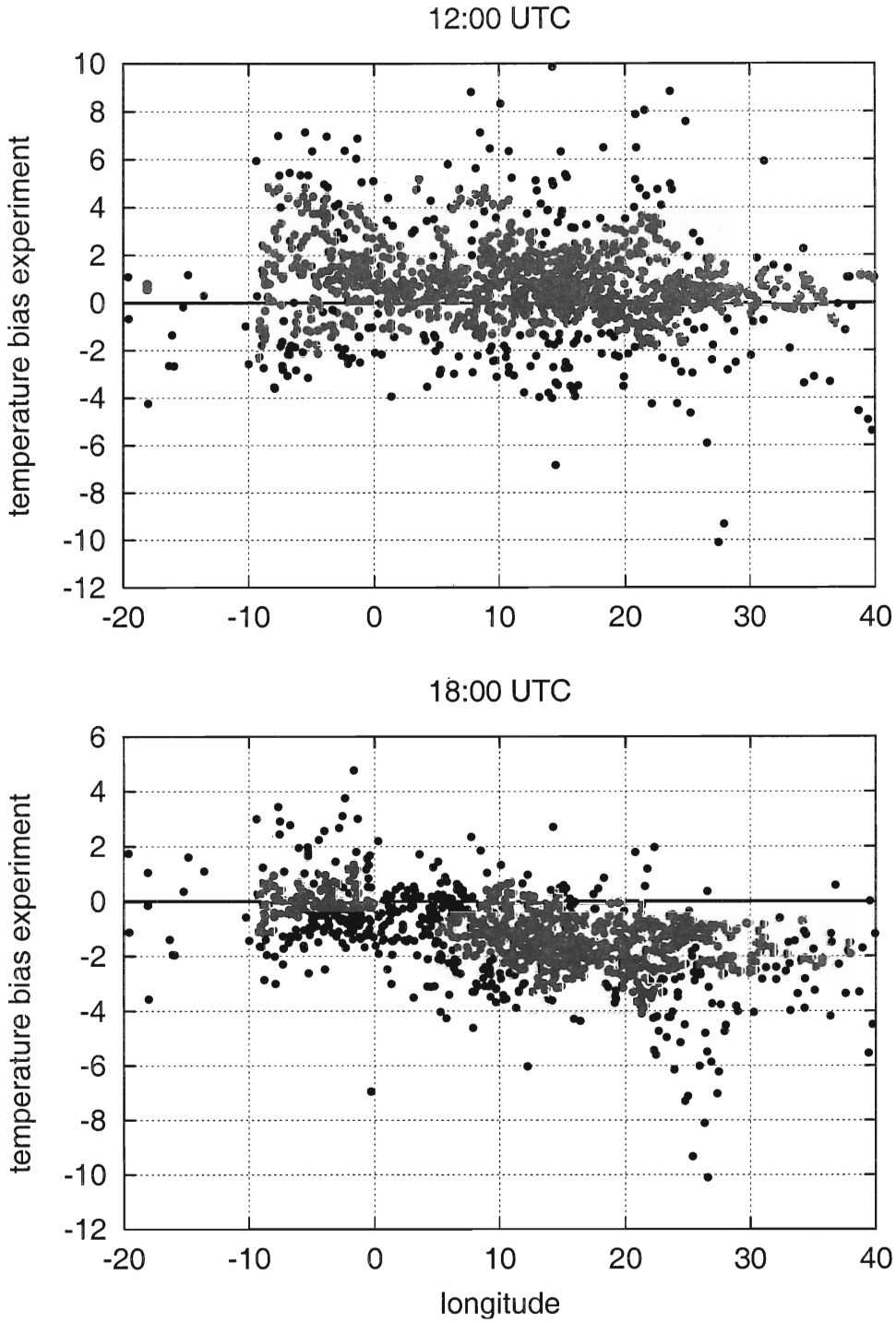

Figure 10: Average temperature bias of the experimental suite in July 2000 for all synops locations plotted as function of the longitude of the measurement location at 12:00 UTC (top panel) and 18:00 UTC (bottom).

The RACMO control run shows a positive 2m temperature bias. The bias points to problems in the surface scheme itself and has already been reported by Viterbo and Courtier (1995) and Christensen et al. (1998). It leads to systematically overestimation of continental drying in summer time. This temperature bias at noon is removed partially when using the satellite data. The impact, however, is rather limited, which is related to the rather conservative estimates of the accuracy of the satellite data as represented by the observation error (Equation 3). More tests would be needed to fine-tune the formulation of this error in relation to the model background error.

The most complicating factor in using satellite-derived heating rates to improve surface fluxes in a land surface

model is the fact that many processes affect the surface temperature and its tendency. The difference in performance of the scheme between Central Europe and the Iberian Peninsula (Figure 7) is probably to some extend related to how the aerodynamic coupling between the surface and the atmosphere is being resolved in the model. The sparsely vegetated surface in the Mediterranean results in different mechanisms for momentum and heat transfer between the surface and the atmosphere, which is reflected in the z_{0h}/z_{0m}-ratio. For instance, an analysis of directional surface temperature data by Van den Hurk et al. (in press) revealed that the optimal z_{0h}/z_{0m}-ratio for e.g. a Spanish vineyard area and a Dutch meadowland are much lower than the model value used. This may have resulted in overestimating the aerodynamic coupling, leading to surface temperatures changes that are too low. Consequently, the scheme would try to compensate this discrepancy by decreasing the soil moisture content.

The fact that the soil moisture content is not related unambiguously to surface heating rates makes a soil moisture assimilation scheme based on satellite heating rate observations a difficult task. Ideally, apart from soil moisture content also aerodynamic parameters should be optimised to get a good match between modelled and observed quantities. Satellite data alone contain too many degrees of freedom for this exercise, and additional data sources must be applied in conjunction with the satellite temperature data. As proposed by e.g. Shuttleworth (1998), a combination of satellite derived surface temperature, shortwave radiation and microwave data of the top layer soil moisture content provide a much more powerful set of observations for soil moisture assimilation purposes.

Acknowledgements

This study was partially sponsored by the Dutch Committee on Remote Sensing under contract number 4.2/AP-10. Discussions with Arnout Feijt, Pedro Viterbo, Anton Beljaars, Massimo Menenti, Bert Holtslag and Peter Troch on the matter are surely appreciated. The work benefited greatly from the development of the simplified variational assimilation method, kindly provided by Reinhold Hess.

References

Bastiaanssen, W.G.M., H. Pelgrum, P. Droogers, H.A.R. de Bruin and M.Menenti (1997): Area-average estimates of evaporation, wetness indicators and top soil moisture during two golden days in EFEDA;Agricultural and Forest Meteorology 87, 119-137.

Bouttier, F., J.-F. Mahfouf and J. Noilhan (1993a): Sequential assimilation of soil moisture from atmospheric low-level parameters.Part I: Sensitivity and calibration studies; J. Applied Meteorol. 32, 1335-1351.

Bouttier, F., J.-F. Mahfouf and J. Noilhan (1993b): Sequential assimilation of soil moisture from atmospheric low-level parameters.Part II: Implementation in a mesoscale model; J. Applied Meteorol. 32, 1352-1364.

Calvet, J.-C., J. Noilhan and P. Bessemoulin (1998): Retrieving the root-zone soil moisture from surface soil moisture or temperature estimates: a feasibility study based on field measurements; J.Applied Meteorol. 37, 371-386.

Christensen, J.H., O.B. Christensen, P. Lopez, E. van Meijgaard and M. Botzet (1996): The HIRHAM4 Regional Atmospheric Climate Model; Danish Meteorol. Institute, Copenhagen, Scientific Report 96-4, 51 pp.

Christensen, J.H., B. Machenauer, R.G. Jones, C. Schär, P.M. Ruti, M. Castro and G. Visconti (1997): Validation of present-day regional climate simulations over Europe: LAM simulations with observed boundary conditions; Clim. Dyn. 13, 489-506.

Douville, H., P. Viterbo, J.-F. Mahfouf and A.C.M. Beljaars (2000): Evaluation of the optimum interpolation and nudging techniques for soil moisture analysis using FIFE data; Monthly Weather Review 128, 1733-1756.

Feijt, A., P. de Valk and S. van der Veen (2000): Cloud detection using METEOSAT imagery and numerical weather prediction model data; J. Applied Meteorol. 39, 1017-1030.

Giard, D. and Bazile (2000): Implementation of a new assimilation scheme for soil and surface variables in a global NWP model; Monthly

Weather Rev. 128, 997-1015.

Gustafsson, N. (1993): hirlam 2 final report; available from smhi, S-60176 Norrköping, Sweden.

Hess, R. (2001): Assimilation of screen-level observations by variational soil moisture analysis; Meteorol.Atm.Phys. 77, 145-154.

Houser, P., W.J. Shuttleworth, J.S. Famiglietti, H.V. Gupta, K.H. Syed and D.C. Goodrich (1998): Integration of remote sensing and hydrologic modeling using data assimilation; Water Resources Research 34, 3405-3420.

Jones, A.S., I.C. Guch and Th.H. Vonder Haar (1998a): Data assimilation of satellite-derived heating rates as proxy surface wetness data into a regional atmospheric mesoscale model, Part 1: Methodology; Monthly Weather Review 126, 634-645

Jones, A.S., I.C. Guch and Th.H. Vonder Haar (1998b): Data assimilation of satellite-derived heating rates as proxy surface wetness data into a regional atmospheric mesoscale model, Part II: A Case study; Monthly Weather Review 126, 646-667.

Koster, R.D. and M.J. Suarez (1992): Modeling the land surface boundary in climate models as a composite of independent vegetation stands; J.Geophys. Res. (D) 97, 2697-2715.

Koster, R.D., Max J. Suarez, Mark Heiser, 2000: Variance and Predictability of Precipitation at Seasonal-to-Interannual Timescales. Journal of Hydrometeorology: Vol. 1, No. 1, pp. 26-46.

Mahfouf, J.-F. (1991): Analysis of soil moisture from near-surface parameters: a feasibility study; J. Appl. Meteorol. 30, 1534-1547.

McNider, R.T., A.J. Song, D.M. Casey, P.J. Wetzel, W.L. Crosson and R.M. Rabin (1994): Toward a dynamic-thermodynamic assimilation of satellite surface temperature in numerical atmospheric models; Monthly Weather Rev. 122, 2784-2803.

Menenti, M. and B.J. Choudhury (1993): Parameterization of land surface evaporation by means of location dependent potential evaporation and surface temperature range; In: Exchange Processes of the land surface for a range of space and time scales (Proceedings of the Yokohama Symposium, July 1993); IAHS Publ 212, pp. 561-568.

Muller, S.H., H. The, W. Kohsiek and W. Monna (1990): Description of CRAu data set: METEOSAT data, radiosonde data, sea surface temperatures. Comparison of METEOSAT and Heimann data; KNMI Scientific Rep. WR 90-03, KNMI, De Bilt, The Netherlands.

Rhodin, F., F. Kucharski, U. Callies, D. P. Eppel and W. Wergen (1999): Variational analysis of effective soil moisture from screen-level atmospheric parameters; application to a short-range forecast; Q.J.Roy.Met.Soc. 125, 2427-2448.

Shuttleworth, W.J. (1998): Combining remotely sensed data using aggregation algorithms; Hydr. and Earth System Sci. 2, 149-158.

Sun, J. and L. Mahrt (1995): Determination of surface fluxes form the surface radiative temperature; J. Atmos. Sci. 52, 1096-1106.

Van den Hurk, B.J.J.M. (2001): Energy balance based surface flux estimation from satellite data, and its application for soil moisture estimation; Meteorol.Atm.Phys 76, 43-52.

Van den Hurk, B.J.J.M., W. Bastiaanssen, H. Pelgrum and E. van Meijgaard (1997): A new methodology for initialization of soil moisture fields in numerical weather prediction models using METEOSAT and NOAA data; J. Applied Meteorology 36, 1271-1283.

Van den Hurk, B.J.J.M., P. Viterbo, A.C.M. Beljaars and A.K. Betts (2000): Offline validation of the ERA40 surface scheme; ECMWF TechMemo 295; ECMWF, Reading, UK.

Van den Hurk, B.J.J.M., L. Jia, C. Jacobs, M. Menenti and J.-L. Li (in press): Assimilation of land surface temperature data from ATSR uin an NWP environment: a case study; in press by Int.J.Rem.Sens.

Verhoef, A., H.A.R. de Bruin and B.J.J.M. van den Hurk (1997): Some practical notes on the parameter kB-1 for sparse vegetation; J.Applied Meteorol. 36, 560-572.

Viterbo, P., 1996: The representation of surface processes in general circulation models. PhD-thesis, ECMWF, Reading, UK, 201 pp.

Viterbo, P. and A.C.M. Beljaars (1995): An improved land surface parametrization scheme in the ECMWF model and its validation; J.Climate 8, 2716-2748.

Viterbo, P. and P. Courtier (1995): The importance of soil water for medium-range weather forecasting. Implications for data assimilation. WMO workshop on Imbalances of slowly varying components of predictable atmospheric motions, Beijing, China, March 1995; WMO/TD 652, pp. 121-130.

Wetzel, P.J., D. Atlas and R.H Woodward (1984): Determining soil moisture from geosynchronous satellite infrared data: a feasibility study; J. Climate Appl. Meteorol. 23}, 375-391.

Wigneron, J.-P., A. Olioso, J.-C. Calvet and P. Bertuzzi (1999): Estimating root-zone soil moisture from surface soil moisture data and Soil-Vegetation-atmosphere transfer modelling; Water Resources Research 35, 3735-3745.

Wigneron, J.-P., P. Waldteufel, A. Chanzy, J.-C. Calvet and Y. Kerr (2000): Two-dimensional microwave interferometer retrieval capabilities over land surfaces (SMOS Mission); Rem.Sens.Env. 73, 270-282.

OVERZICHT VAN RECENT VERSCHENEN KNMI-PUBLICATIES

KNMI-PUBLICATIE MET NUMMER

186-II Rainfall generator for the Rhine Basin: multi-site generation of weather variables by nearest-neighbour resampling / T. Brandsma a.o.

186-III Rainfall generator for the Rhine Basin: nearest-neighbour resampling of daily circulation indices and conditional generation of weather variables / Jules J. Beersma and T. Adri Buishand

186-IV Rainfall generator for the Rhine Basin: multi-site generation of weather variables for the entire drainage area / Rafal Wójcik, Jules J. Beersma and T. Adri Buishand

189 Aardbevingen in Noord-Nederland in 1998: met overzichten over de periode 1986-1998 / [Afdeling SO]

190 Seismisch netwerk Noord-Nederland / [afdeling Seismologie]

191 Het KNMI-programma HISKLIM (HIStorisch KLIMaat) / T. Brandsma, F. Koek, H. Wallbrink, G. Können

192 Gang van zaken 1940-48 rond de 20.000 zoekgeraakte scheepsjournalen / Hendrik Wallbrink en Frits Koek

193 Science requirements document for OMI-EOS / contr. by R. van der A .. [et al.] **(limited distribution)**

194-1 De zonsverduistering van 11 augustus 1999, deel 1: de waarnemingen van het gedrag van flora en fauna / J. Kuiper, m.m.v. Guus Kauffeld

195 An optimal infrasound array at Apatity (Russian Federation) / Läslo Evers and Hein Haak **(limited distribution)**

196-I Rainfall Generator for the Meuse Basin: simulation of 6-hourly rainfall and temperature for the Ourthe catchment / Rafal Wójcik and T. Adri Buishand

197 Meteorologie op zee: beknopte handleiding voor waarnemingen op zee [= manual meteorology at sea] **(limited distribution)**

TECHNISCH RAPPORT = TECHNICAL REPORT (TR)

227 Seismo-akoestische analyse van de explosies bij *S.E. Fireworks* ; Enschede 13 mei 2000 / L.G. Evers e.a.

228 Evaluation of modified soil parameterization in the ECMWF landsurface scheme / R.J.M. IJpelaar

229 Evaluation of humidity and temperature measurements of Vaisala's HMP243 plus PT100 with two reference psychrometers / E.M.J. Meijer

230 KNMI contribution to the European project WRINCLE: downscaling relationships for precipitation for several European sites / B.-R. Beckmann and T.A. Buishand

231 The Conveyor Belt in the OCCAM model: tracing water masses by a Lagrangian methodology / Trémeur Balbous and Sybren Drijfhout

232 Analysis of the Rijkoort-Weibull model / Ilja Smits

233 Vectorization of the ECBilt model / X. Wang and R.J. Haarsma

234 Evaluation of a plant physiological canopy conductance model in the ECMWF land surface scheme / J. van de Kassteele

235 Uncertainty in pyranometer and pyrheliometer measurements at KNMI in De Bilt / J.S. Henzing a.o.

236 Recalibration of GOME spectra for the purpose of ozone profile retrieval / Ronald van der A

237 Tracing water masses in the Atlantic / Yann Friocourt and Siebren Drijfhout

238 Klimaat voor Amsterdam Airport Schiphol / A. Smits

239 Seismische analyse van de aardbevingen bij Alkmaar op 9 en 10 september en Bergen aan Zee op 10 oktober 2001 / H.W. Haak, B. Dost, F.H. Goutbeek

240 EBEX-2000 : the KNMI/WAU contribution / W. Kohsiek, E.W. Meijer, P.J.B. Versteeg, O.K. Hartogensis, a.o.

241 Ontwikkeling gidsvergelijkingen voor meerdaagse neerslagkansen / D. Vogelezang en K. Kok

242 On photosynthesis parameters for the A-gs surface scheme for high vegetation / G.J. Steeneveld

243 Temperatuurvergelijkingen voor de Middellange Termijn Gids : ontwikkeling en verificatie over 2000 / J.Wijngaard

244 Verification of clear-air turbulence forecasts / A. Overeem

245 A comprehensive description of the KNMI seismological instrumentation / B. Dost and H. Haak

WETENSCHAPPELIJK RAPPORT = SCIENTIFIC REPORT (WR)

00-03 Salmon's Hamiltonian approach to balanced flow applied to a one-layer isentropic model of the atmosphere / W.T.M. Verkley

00-04 On the behaviour of a few popular verification scores in yes-no forecasting / C.J. Kok

01-01 Hail detection using single-polarization radar / Iwan Holleman

01-02 Comparison of modeled ozone distributions with ozonesonde observations in the tropics / Rob Put

01-03 Impact assessment of a doppler wind lidar in space on atmospheric analyses and numerical weather prediction / G.J. Marseille, A. Stoffelen, F. Bouttier, C. Cardinali, S. de Haan and D. Vasiljevic.

02-01 Quality control and wind retrieval for SeaWinds / M. Potabella and A. Stoffelen

02-02 Shortwave radiation and cloud parameterizations for intermediate complexity models / J.J. Beersma, R. van Dorland and J.D. Opsteeg

02-03 Sensitivity study of the residue method for the detection of aerosols from space-borne sensors / M. de Graaf

02-04 Assimilation of satellite derived surface heating rates in a Numerical Weather Prediction model / Bart van den Hurk and Han The.

KNMI Bibliotheek, postbus 201, 3730 AE De Bilt, tel. 030 - 2 206 855, fax 030 - 2 210 407; bibliotheek@knmi.nl